JES
JOURNAL OF ENVIRONMENTAL SCIENCES
www.jesc.ac.cn

Shape dependence of support for NO$_x$ storage and reduction catalysts

Wen Xie[1,2], Yunbo Yu[1,2,3,*], Hong He[1,2,3,*]

1. State Key Joint Laboratory of Environment Simulation and Pollution Control, Research Center for Eco-Environmental Sciences, Chinese Academy of Sciences, Beijing 100085, China
2. University of Chinese Academy of Sciences, Beijing 100049, China
3. Center for Excellence in Regional Atmospheric Environment, Institute of Urban Environment, Chinese Academy of Sciences, Xiamen 361021, China

ARTICLE INFO

ABSTRACT

Pt/BaO/Al$_2$O$_3$ catalysts with different BaO loadings prepared from Al$_2$O$_3$ nanorods (Pt/BaO/Al$_2$O$_3$-nr) and irregular Al$_2$O$_3$ nanoparticles (Pt/BaO/Al$_2$O$_3$-np) were investigated for NO$_x$ storage and reduction (NSR). The Pt/BaO/Al$_2$O$_3$ materials derived from Al$_2$O$_3$ nanorods always exhibited much higher NO$_x$ storage capacity (NSC) over the whole temperature range of 100–400°C than the corresponding Pt/BaO/Al$_2$O$_3$-np samples containing the same BaO loading, giving the maximum NSC value of 966.9 μmol/g$_{cat}$ at 400°C, 1.4 times higher than that of Pt/BaO/Al$_2$O$_3$-np. Higher catalytic performance of nanorod-supported NSR samples was also observed during lean-rich cyclic conditions (90 sec *vs.* 5 sec), giving more than 98% NO$_x$ conversion at 300–450°C over the Pt/BaO/Al$_2$O$_3$-nr sample with 15% BaO loading. To reveal this dependence on the shape of the support during the NSR process, a series of characterization techniques including the Brunauer–Emmett–Teller (BET) method, X-ray diffraction (XRD), X-ray photoelectron spectroscopy (XPS), H$_2$ temperature programmed reduction (H$_2$-TPR), and *in situ* diffuse reflectance infrared Fourier transform spectroscopy (DRIFTS) were also conducted. It was found that intimate contact of Ba–Al and Ba–Pt sites was achieved over the Pt/BaO/Al$_2$O$_3$ surface when using Al$_2$O$_3$-nr as a support. This strong interaction among the multi-components of Pt/BaO/Al$_2$O$_3$-nr thus triggered the formation of surface nitrite and nitrate during the lean period, and also accelerated the reverse spillover of ad-NO$_x$ species onto the Pt surface, enhancing their reduction and leading to high NSR performance.

© 2018 The Research Center for Eco-Environmental Sciences, Chinese Academy of Sciences. Published by Elsevier B.V.

Introduction

By virtue of their highly efficient fuel economy and low carbon dioxide emissions (Kašpar et al., 2003), lean burn engines are considered the promising options for tackling the world's growing energy crisis and contributing to preventing climate change (Burch, 2011). For lean burn engines, a large amount of oxygen is present in the exhausts. Under these conditions, the widely accepted three-way catalyst cannot effectively eliminate nitrogen oxides (NO$_x$) (Matsumoto, 2004). Therefore, development of new technologies with high efficiency for lean burn NO$_x$ removal has attracted much attention in recent decades. To this aim, NO$_x$ storage reduction (NSR) working under lean-rich cycling conditions, as one of the most promising technologies,

---

* Corresponding authors. E-mail: ybyu@rcees.ac.cn, (Yunbo Yu), honghe@rcees.ac.cn. (Hong He).

was first proposed and developed by Toyota Corporation in the mid-1990s (Miyoshi et al., 1995). During the lean phase, NO, as the main component of NO_x in lean burn engine exhaust, is oxidized and stored as nitrites and nitrates on the surface of the NSR catalysts. When switching to the rich phase, the stored NO_x is released and then reduced to N_2 (Epling et al., 2004; Liu and Gao, 2011; Liu and Woo, 2006; Roy and Baiker, 2009).

Generally, NSR catalysts mainly contain noble metals (e.g., Pt, Pd, Rh (Clayton et al., 2009; Kim et al., 2008; Say et al., 2014)) for NO oxidation and adsorbed NO_x reduction, alkali or alkaline earth metals (e.g., Ba, Mg, K (Cui et al., 2017; Kim et al., 2013; Zhang et al., 2015)) for NO_x storage and a high-surface-area support material (e.g., γ-Al_2O_3, CeO_2 (Lv et al., 2013; Wang et al., 2011)). Among the developed NSR catalysts, Pt/BaO/Al_2O_3, as the classical example, exhibits high efficiency for NO_x removal within the temperature range of 250–400°C (Epling et al., 2004; Hu et al., 2013; Roy and Baiker, 2009; Wang et al., 2010). To further improve its catalytic performance, meanwhile, many studies have been devoted to addressing the catalytic role of the various components contained in this sample and the reaction steps occurring in the NSR process. The oxidation of NO to NO_2 in the lean condition, as a key step for NO_x storage, mainly occurs over the Pt sites of Pt/BaO/Al_2O_3. In this case, the dispersion and availability of active Pt species (such as metal Pt particles with suitable size) are crucial for achieving a high reaction rate for NO oxidation (Anderson et al., 2003; Bhatia et al., 2009; Olsson and Fridell, 2002). By quantitative analysis of the relationship between Ba coverage and NO_x storage capacity (NSC), Castoldi et al. (2004) found that Pt/BaO/Al_2O_3 with moderate Ba loading of ca. 23 wt.% gave the highest NSC value. Such Ba loading dependence of NO_x storage was also revealed by Piacentini et al. (2005), based on addressing the build-up, stability and reactivity of Ba-containing phases present in Pt/BaO/Al_2O_3. On the NSR sample with moderate Ba loading, indeed, Ba-containing phases neighboring Pt sites and/or interacting intimately with the alumina support were dominant, benefiting the spillover of ad-NO_x species (nitrite and nitrate), and finally relating to the NO_x storage process (Castoldi et al., 2004; Piacentini et al., 2005; Zhou et al., 2006). Furthermore, experimental and theoretical studies confirmed that the strong interaction between BaO and penta-coordinated Al^{3+} present on the surface of alumina was beneficial for nitrate formation, accelerating the NO_x storage process (Kwak et al., 2007, 2009; Yi et al., 2007).

The achievements mentioned above unambiguously revealed that intimate contact among the multi-components of Pt/BaO/Al_2O_3 is important for NO oxidation and its further storage. Also, such strong interaction was found to be crucial for NO_x reduction occurring in the rich period of the NSR process (Maeda et al., 2011), considering that the ad-NO_x desorption from Ba and Al components should undergo reverse spillover onto the Pt surface (Anderson et al., 2003; Hu et al., 2013). As expected, more recently, Pt/BaO/Al_2O_3 catalysts with high NSR efficiency were created by tuning the Ba precursor (Maeda et al., 2011), and by pre-calcination of the alumina support (Hu et al., 2013).

As for supported catalysts, it should be noted that numerous studies have demonstrated that the morphology of the employed support on the nano-scale profoundly affects the active phase and thus the catalytic performance (Huang et al., 2017; Li and Shen, 2014; Rao et al., 2018; Wang et al., 2016; Zhou

and Li, 2012). In our previous study, such shape dependence was also confirmed during the NO_x storage reduction process by using CeO_2 nanomaterials with different shapes as the supports of NSR catalysts (Zhang et al., 2016). To the best of our knowledge, however, there has been little information focusing on the effect of the morphology of alumina on the catalytic performance of Pt/BaO/Al_2O_3. To address this issue, herein, Al_2O_3 nanorods and Al_2O_3 particles with irregular shape were employed as the supports for synthesis of NSR catalysts. Based on characterization results of the Brunauer–Emmett–Teller (BET) method, X-ray diffraction (XRD), X-ray photoelectron spectroscopy (XPS), H_2 temperature programmed reduction (H_2-TPR), and in situ diffuse reflectance infrared Fourier transform spectroscopy (DRIFTS), it was found that intimate contact among the multi-components of the NSR catalyst was present over Pt/BaO/Al_2O_3 derived from the alumina nanorods, which contributed to high NO_x storage capacity and excellent NO_x reduction behavior during lean-rich cycling conditions.

1. Materials and methods

1.1. Catalyst preparation

Pt/BaO/Al_2O_3 catalysts were prepared via the impregnation method using γ-Al_2O_3 nanorods (Aladdin) and particles (Sigma-Aldrich) as supports, respectively. Specifically, the γ-Al_2O_3 was impregnated in a mixed solution of $Ba(CH_3COO)_2$ and $PtCl_4$. After stirring for 60 min, the excess water was removed in a rotary evaporator at 50°C. The samples were then dried at 100°C overnight and calcined at 500°C for 3 hr in air to obtain the final Pt/BaO/Al_2O_3 catalysts with 1 wt.% Pt loading and 8 wt.%–20 wt.% BaO loading. The catalysts obtained using Al_2O_3 nanorods and irregular particles are hereafter denoted as Pt/nBaO/Al_2O_3-nr (n = 8, 15, or 20 wt.%) and Pt/nBaO/Al_2O_3-np (n = 8, 15, or 20 wt.%), respectively. For H_2-TPR characterization, samples of Pt/Al_2O_3-nr, Pt/Al_2O_3-np, 8 wt.% BaO/Al_2O_3-nr and 8 wt.% BaO/Al_2O_3-np were also prepared with the same procedures as described above.

1.2. Characterization

High-resolution transmission electron microscopy (HRTEM) images were taken on a multi-purpose transmission electron microscope (JEM 2100 PLUS TEM, JEOL, Japan) with 200 kV acceleration voltage. Powder XRD measurements of the catalysts were carried out on a computerized diffractometer (D8 ADVANCE, Bruker, Germany) with a Cu Kα radiation source (λ = 0.15406 nm). The patterns were taken over the 2θ range from 10 to 90° at a step of 0.02°. The specific surface areas of the catalysts were obtained at −196°C over the whole range of relative pressures, using an automatic instrument (Quantasorb-18, Quanta Chrome Instrument Co., USA). Prior to N_2 physisorption, the catalysts were degassed at 300°C for 5 hr. Specific surface areas were calculated from these isotherms by applying the BET equation in the 0.05–0.3 partial pressure range. XPS was conducted using an imaging X-ray photoelectron spectrometer (Axis Ultra, Kratos Analytical Ltd., Japan) with Al Kα radiation. The C 1s peak (binding energy = 284.8 eV) was used as the standard for binding energy calculations.

H_2-TPR was carried out in a fully automated chemisorption analyzer (AutoChem II 2920, Micromeritics, USA), monitored by a thermal conductivity detector (TCD). The samples were pretreated at 450°C in air flow (50 mL/min) for 30 min and cooled down to 50°C. Then reduction profiles were taken by passing a flow of 10% H_2/Ar (50 mL/min) through the sample bed, during which the temperature was increased from 50 to 900°C with a ramp rate of 10°C/min.

In-situ DRIFTS were measured on a Fourier transform infrared spectrometer (Nicolet Nexus 670, Thermo, USA) with a smart collector and an MCT/A detector cooled with liquid nitrogen. Every sample was pretreated in a flow of 3% H_2/N_2 (300 mL/min) at 450°C for 1 hr, and then cooled down to 300°C. A lean-burn gas mixture (500 ppmV NO, 8% O_2, and N_2 balanced) at a rate of 300 mL/min was used to measure the behavior of the NSR catalyst in the NO_x storage progress, and a rich-burn gas mixture (1% H_2/N_2) at a rate of 100 mL/min was used to investigate the ad-NO_x activity. All spectra presented here were recorded by accumulating 30 scans with a resolution of 4 cm^{-1}.

1.3. Catalytic activity measurements

NO_x uptake experiments were carried out under fuel-lean conditions as a function of temperature. Before each experiment, the catalyst was pretreated in 3% H_2/N_2 for 1 hr at 450°C, and then cooled to the desired temperature. A mixed gas (500 ppmV NO, 8% O_2, and N_2 balance) at a total flow rate of 300 mL/min was used to simulate the fuel-lean exhaust. The outlet NO_x (NO + NO_2) concentration was recorded by a chemiluminescence detector (CLD 62, ECO Physics, Switzerland).

NSR cyclic experiments were performed with 100 mg of catalyst. The reactor was connected to a pneumatically actuated four-way valve, which achieved the quick switching between the lean and rich gas. Constant flows (300 mL/min) of (500 ppmV NO +8% O_2) and (500 ppmV NO +3% H_2) were introduced alternately, during which a lean period for 90 sec and a rich period for 5 sec were applied between 100 and 450°C. The average NO_x conversion was calculated over 20 lean/rich cycles Eq. (1):

$$NO_x \text{ conversion} = \frac{NO_{x,in} - NO_{x,out}}{NO_{x,in}} \times 100\% \qquad (1)$$

where $NO_{x,in}$ (ppmV) and $NO_{x,out}$ (ppmV) are the concentration of inlet flow and outlet flow, respectively.

2. Results and discussion

2.1. Structural features

The morphology of Pt/BaO/Al_2O_3 catalysts was characterized by HRTEM, with typical images shown in Fig. 1. The Pt/8%BaO/Al_2O_3-nr displayed a nanorod shape, with diameter of ca.5 nm and length of 30–60 nm (Fig. 1b), which is similar to that of pure Al_2O_3-nr (Fig. 1a). Increasing the BaO loading to 15 wt.% resulted in the aggregation of alumina, while maintaining the original crystal shape with an increased diameter (Fig. 1c). Such aggregation was more serious when BaO loading was raised to 20 wt.% (Fig. 1d), presenting irregular sheets together

with the initial nanorod shape. As shown in Fig. 1e, the Al_2O_3-np sample was in the form of irregularly shaped particles. Similar to nanorod-based NSR catalysts, high BaO loading also induced pronounced aggregation of samples derived from Al_2O_3-np (Fig. 1f–h).

The BET surface areas of the Al_2O_3 supports and corresponding NSR catalysts are presented in Table 1. Pure Al_2O_3-np had a larger surface area (176.9 m^2/g) than Al_2O_3-nr (128.8 m^2/g). BaO loading resulted in a decrease in the BET surface area. The higher the BaO loading, the smaller the surface area of the catalysts was, possibly due to the aggregation of samples/supports as shown in Fig. 1. For a given BaO loading, it should be noted that the Pt/BaO/Al_2O_3-np sample always had a larger surface area than the corresponding one prepared from Al_2O_3-nr.

The crystal structures of the NSR samples were measured by XRD (Fig. 2). As can be seen in the figure, the diffraction peaks ascribed to alumina (JCPDS no. 16-0394) and $BaCO_3$ (JCPDS no. 44-1487) were observed in all the NSR samples, while no peaks assignable to Pt species were detected in any of the samples, indicating high dispersion of this component. Compared with Al_2O_3-np, pure Al_2O_3-nr showed higher crystallinity. After Ba and Pt loading, also, the Al_2O_3-nr related NSR catalysts contained $BaCO_3$ with higher crystallinity. Using the Scherrer equation for the peak at $2\theta = 23.9°$, furthermore, the $BaCO_3$ crystal sizes of the NSR samples were calculated (Table 1). For a given Ba content, interestingly, the size of $BaCO_3$ particles supported on Al_2O_3-nr was always smaller than that on Al_2O_3-np, strongly suggesting that using Al_2O_3-nras support is beneficial for the distribution of the Ba-containing phase. For a given Al_2O_3 support, it should be noted that the calculated $BaCO_3$ crystal size decreased with the increase of BaO loading (Table 1). Generally, an increase of BaO loading would be expected to result in an increased crystal size for $BaCO_3$. As suggested by Piacentini et al. (2005), however, $BaCO_3$ with monoclinic and orthorhombic phases appeared as the Ba-loading increased from 16 to 22 wt.%, and the relative amount of the latter increased proportionally to the Ba loading. The orthorhombic $BaCO_3$ present on the outermost layer of the catalyst had a higher degree of crystallinity than the monoclinic phase. To accurately calculate the particle size of $BaCO_3$, therefore, the different phases of Ba-containing species and their amounts should be considered carefully.

2.2. Catalytic performance

2.2.1. NO_x storage performance
The NO_x storage behavior of all the NSR samples within the temperature range of 100–400°C is shown in Appendix A Fig. S1. Once a sample was exposed to the lean feed, the concentration of NO_x in the outlet gas dropped sharply from 500 to 0 ppmV, followed by a process of complete uptake. With increased time, the NO_x concentration in the outlet increased gradually, achieving a saturation state after ca. 3600 sec. Based on the breakthrough curves presented in Appendix A Fig. S1, the NO_x storage capacities (NSC) were calculated and summarized in Fig. 3. For a given sample, a higher reaction temperature often results in a larger NSC value. Over all the samples, generally, increased BaO loading induced an increase in NSC values,
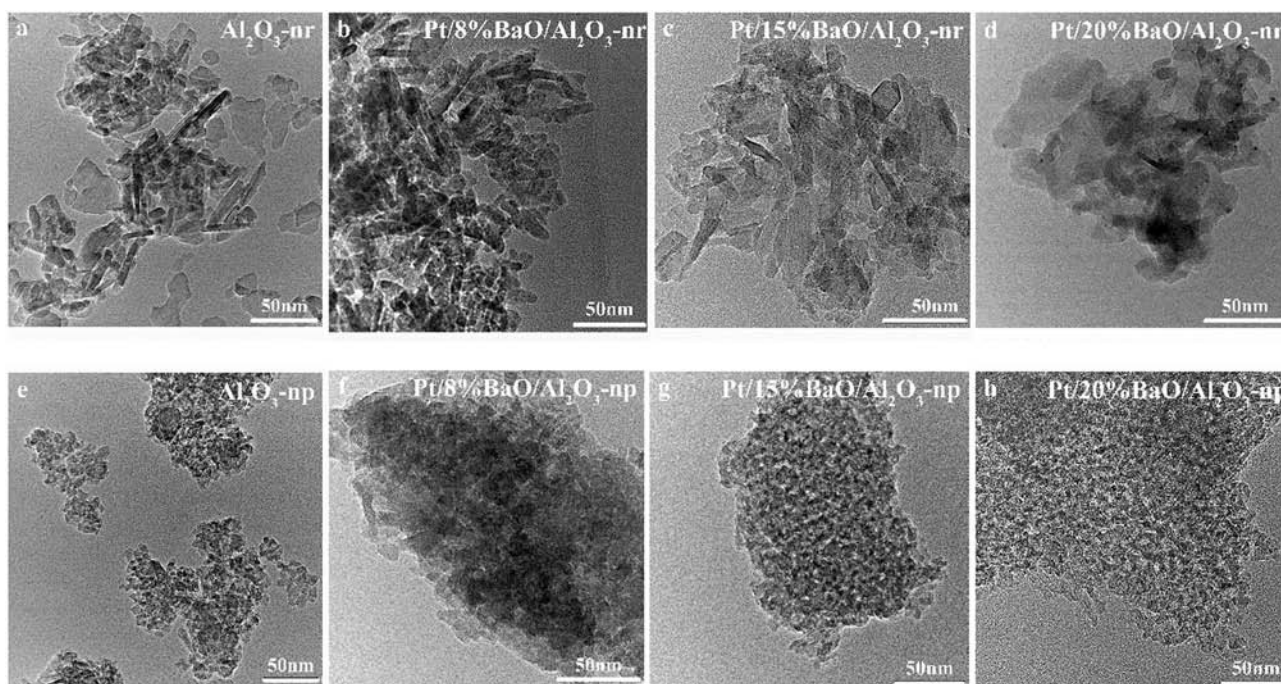
Fig. 1 – High resolution transmission electron microscopy (HRTEM) of (a) Al_2O_3-nr, (b) Pt/8%BaO/Al_2O_3-nr, (c) Pt/15%BaO/Al_2O_3-nr, (d) Pt/20%BaO/Al_2O_3-nr, (e) Pt/Al_2O_3-np, (f) Pt/8%BaO/Al_2O_3-np, (g) Pt/15%BaO/Al_2O_3-np, and (h) Pt/20%BaO/Al_2O_3-np. The marks of nr and np refer to nanorods and nanoparticles, respectively.

particularly for the samples derived from Al_2O_3-nr. In the case of the samples with the same BaO loading, it is very interesting that the Pt/BaO/Al_2O_3-nr showed much larger NSC than Pt/BaO/ Al_2O_3-np at all temperatures tested. At the temperature of 400°C, Pt/15%BaO/Al_2O_3-nr exhibited NSC of 558.9 μmol/g_{cat}, ca. 50% higher than that of the Al_2O_3-np related sample. As for the samples containing 20 wt.% BaO, the NSC of Pt/BaO/Al_2O_3-nr was up to 966.9 μmol/g_{cat} at 400°C, 1.4 times higher than of Pt/BaO/Al_2O_3-np, indicating a strong support shape effect.

It has been widely accepted that the oxidation of NO to NO_2 is a crucial step for NO_x storage, the occurrence of which is significantly promoted by platinum (Anderson et al., 2003; Fridell et al., 2000). To highlight this issue, the ratio of $NO_2/(NO + NO_2)$ at the end of the storage period was calculated

and shown in Appendix A Fig. S2. For a given Pt/BaO/Al_2O_3 material, particularly for samples derived from Al_2O_3-nr, a high $NO_2/(NO + NO_2)$ always related to an increased NO_x storage capacity at temperatures below 300°C, confirming the crucial role of NO oxidation (Bhatia et al., 2009; Castoldi et al., 2004; Olsson and Fridell, 2002). With this in mind, it is reasonable that Pt/BaO/Al_2O_3-nr exhibits a higher NSC value than the corresponding Pt/BaO/Al_2O_3-np material with the same BaO loading due to the higher oxidation ability of the former. At a given

Table 1 – Brunauer–Emmett–Teller (BET) surface area and $BaCO_3$ crystal size of the Al_2O_3 supports and Pt/nBaO/ Al_2O_3 catalysts.

Samples	BET (m^2/g)	$BaCO_3$ size (nm)
Al_2O_3-np	176.9	–
Pt/8%BaO/Al_2O_3-np	143.3	39.4
Pt/15%BaO/Al_2O_3-np	117.2	30.4
Pt/20%BaO/Al_2O_3-np	108.2	29.6
Al_2O_3-nr	128.8	–
Pt/8%BaO/Al_2O_3-nr	120.5	32.0
Pt/15%BaO/Al_2O_3-nr	104.4	23.6
Pt/20%BaO/Al_2O_3-nr	101.7	21.0

$BaCO_3$ size was calculated based on the $BaCO_3$ diffraction peak at $2\theta = 23.9°$ by applying the Scherrer equation.
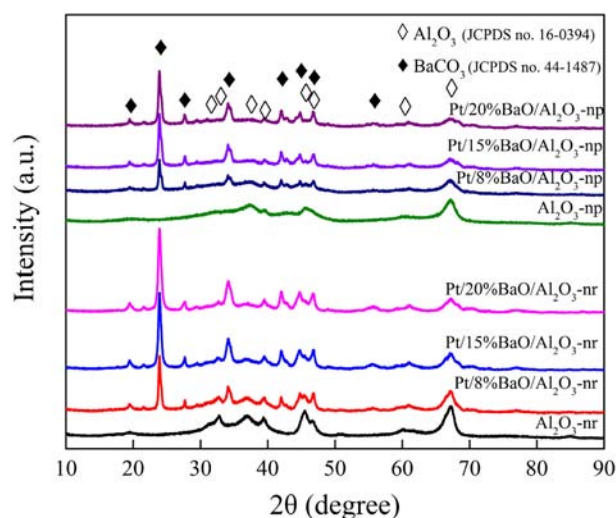
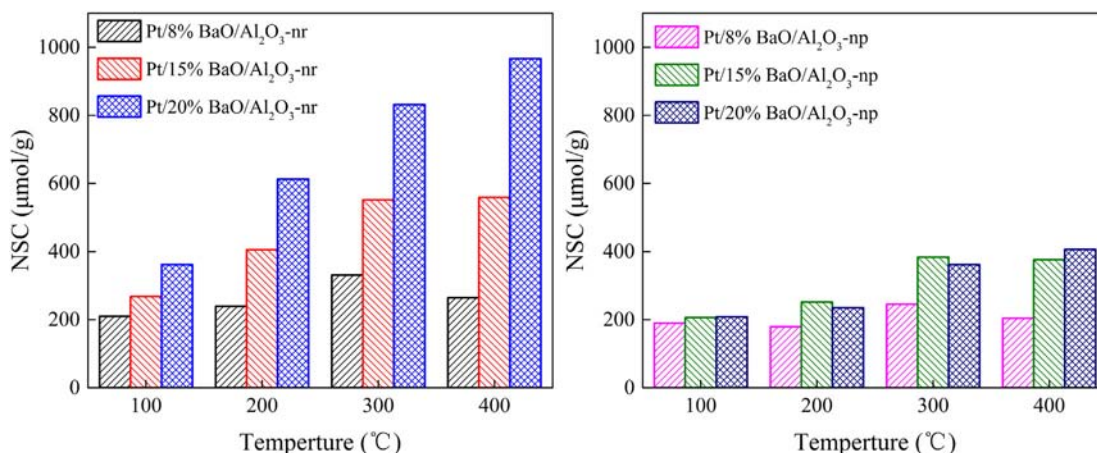**Fig. 2 – X-ray diffraction (XRD) patterns of Al_2O_3 supports and Pt/BaO/Al_2O_3 samples.**

Fig. 3 – NO$_x$ storage capacities (NSC) tested at different temperatures over Pt/BaO/Al$_2$O$_3$-nr and Pt/BaO/Al$_2$O$_3$-np catalysts.

temperature, it should be noted that higher BaO loading often results in a lower ratio of NO$_2$/(NO + NO$_2$), indicating a negative effect of Ba on NO oxidation (Castoldi et al., 2004; Olsson and Fridell, 2002; Olsson et al., 2001).

*2.2.2. Dynamic NO$_x$ storage and reduction performance*
As for the actual operation of NSR application, a few seconds of rich combustion reduction time and a NO$_x$ storage process operating at the minute-scale are usually employed to improve fuel efficiency (Roy and Baiker, 2009). Following this practice, in this study, the NO$_x$ removal efficiency of NSR catalysts was evaluated with a 90 sec lean period and a rich period of 5 sec with a space velocity (SV) of 180,000 mL/(g·hr), by using hydrogen as a reducing agent (Hussam et al., 2004, 2006; Maeda et al., 2009; Wang et al., 2010).

During the rich phase, the reduction of ad-NO$_x$ over Pt/BaO/Al$_2$O$_3$was assumed to take place as follows:

$$Ba(NO_3)_2 + 5H_2 \rightarrow N_2 + BaO + 5H_2O$$
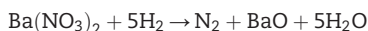
Supposing all NO$_x$ was trapped as Ba(NO$_3$)$_2$, 25 μmol H$_2$ needed to be introduced in the lean phase for complete reduction of 10 μmol NO$_x$. However, NO$_x$ also existed in the feed gas under rich conditions, and the reduction proceeded as:

$$2NO + 2H_2 \rightarrow N_2 + 2H_2O$$
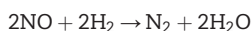
Thus, another 0.6 μmol H$_2$ was required to completely reduce NO in the rich gas phase (Wang et al., 2010). During the 5 sec regeneration period, in this study, 33.5 μmol H$_2$ (3% H$_2$) was introduced to the system, which is about 1.3 times the calculated amount required to reduce all introduced NO$_x$ (Clayton et al., 2009; Zhang et al., 2015).

Taking Pt/15%BaO/Al$_2$O$_3$-nr and Pt/15%BaO/Al$_2$O$_3$-np as representative samples, the real-time behavior of NO$_x$ in the outlet feed of the initial 20 lean/rich cycles at temperatures between 100 and 450°C is given in Fig. 4a and b. Additionally, more details for other samples can be seen in Appendix A

Fig. S3. In agreement with the designed reaction process, all the samples trapped NO$_x$ under the lean condition, coinciding with the uptake curve as shown in Appendix A Fig. S1, and regenerated under the rich condition (Liu and Gao, 2011). At the low temperature of 100°C, complete uptake of NO$_x$ in each lean phase hardly occurred over the Pt/15% BaO/Al$_2$O$_3$-nr (Fig. 4a), possibly due to a lower reaction rate for NO oxidation (Appendix A Fig. S2). At this temperature, however, no NO$_x$ spilled out during the rich period, indicating excellent NO$_x$ reduction performance. Similar uptake and reduction behaviors of NO$_x$ were also observed at the elevated temperature of 150°C, while the adsorption process that occurred in the lean phase became more efficient. Further increasing the reaction temperature to 200°C, complete uptake of NO$_x$ was achieved during all lean periods, while a sharp NO$_x$ spike (~380 ppmV) occurred in each rich phase and then decreased quickly to a low value. This distinct peak during cycle transition has been commonly reported by earlier publications and is thought to be caused by the difference in the reaction rates of nitrate decomposition and NO$_x$ reduction (Epling et al., 2007; Ji et al., 2008; Zhang et al., 2016). With temperature increasing, the intensity of the NO$_x$ spike decreased gradually, and almost disappeared at temperatures between 350 and 400°C. Such NO$_x$ evolution features also appeared over Pt/15%BaO/Al$_2$O$_3$-np, while showing a much stronger NO$_x$ spike (~560 ppmV at 250°C) compared with those of Pt/15%BaO/Al$_2$O$_3$-nr at a given temperature, indicating lower NO$_x$ reduction performance. Also, this support morphology dependence can be easily found by comparison of the average NO$_x$ conversion values over 20 lean/rich cycles (Fig. 4c and d). Within the whole temperature range, the average NO$_x$ conversion achieved on the Pt/15%BaO/Al$_2$O$_3$-nr samples was always ca. 10% higher than that on the Pt/15%BaO/Al$_2$O$_3$-np samples. Clearly, the Pt/15%BaO/Al$_2$O$_3$-nr catalyst afforded excellent NO$_x$ removal efficiency, reaching above 98% at temperatures between 300 and 450°C. Such high efficiency for NO$_x$ removal under lean-rich conditions was also observed on Pt/20%BaO/Al$_2$O$_3$-nr, while the related sample with 8 wt.% BaO loading gave much lower activity at temperatures above 150°C (Fig. 4c). As for the catalysts derived from Al$_2$O$_3$-np (Fig. 4d), in contrast, higher BaO loading often resulted in higher average NO$_x$ conversion.
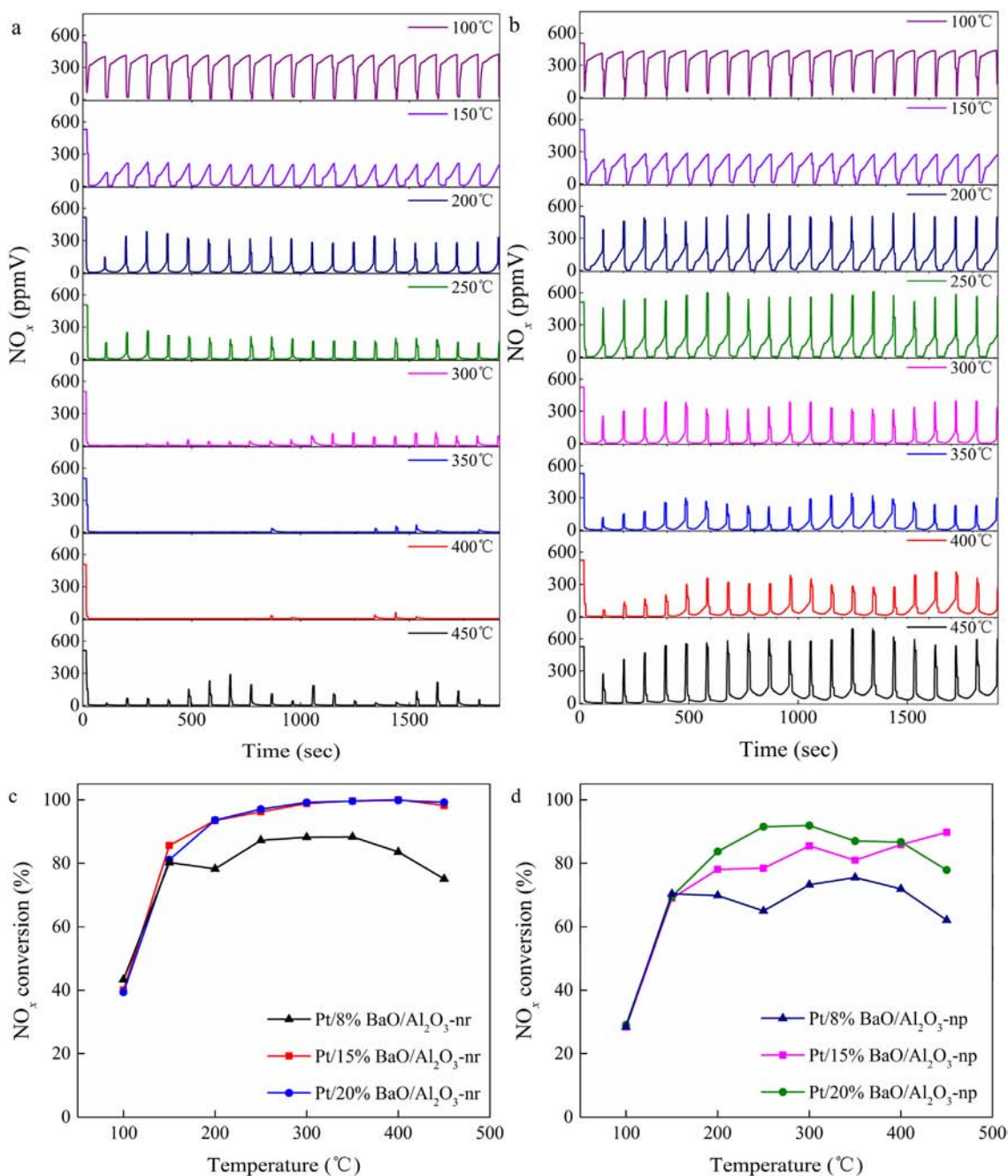
Fig. 4 – Evolution of NO$_x$ concentrations under cyclic lean–rich conditions at different temperatures on (a) Pt/15%BaO/Al$_2$O$_3$-nr and (b) Pt/15%BaO/Al$_2$O$_3$-np; average NO$_x$ conversion over all NSR catalysts under cyclic lean–rich conditions at different temperatures on (c) Pt/nBaO/Al$_2$O$_3$-nr and (d) Pt/nBaO/Al$_2$O$_3$-np.

2.3. Chemical states and redox properties

To reveal the effect of the support on the NSR process, XPS analysis of Pt and Ba was performed for all the NSR samples. Considering the overlap between Al 2p and Pt 4f (Olsson and Fridell, 2002), the characteristic peaks of Pt 4d were measured and presented in Fig. 5. A previous study showed that Pt 4d 3/2 and Pt 4d5/2 for Pt in the metallic state exhibited the binding energies of 331 and 314.6 eV, respectively (Amberntsson et al., 2003). After oxidation, the Pt doublet shifted toward higher binding energies, appearing at 332.8 and 317.3 eV, respectively (Amberntsson et al., 2003). It was also reported that loading of Pt onto the alumina support resulted in a shift of the Pt peaks toward higher values by ca. 0.5 eV (Olsson and Fridell, 2002). For all the Pt/BaO/Al$_2$O$_3$ samples (Fig. 5), the Pt 4d showed peaks at 332.5 and 315.5 eV, with similar intensity. This result
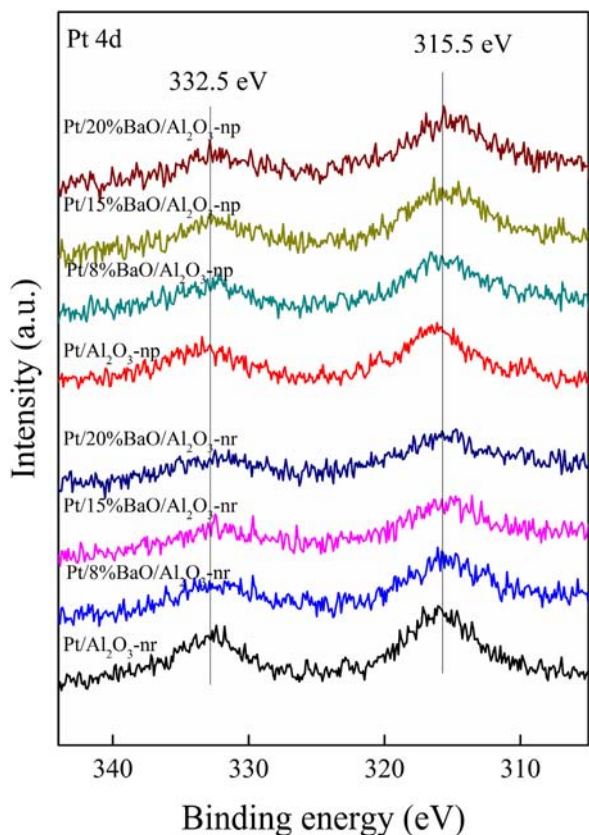
Fig. 5 – X-ray photoelectron spectroscopy (XPS) Pt 4d spectra for Pt/Al$_2$O$_3$ and Pt/BaO/Al$_2$O$_3$ catalysts.
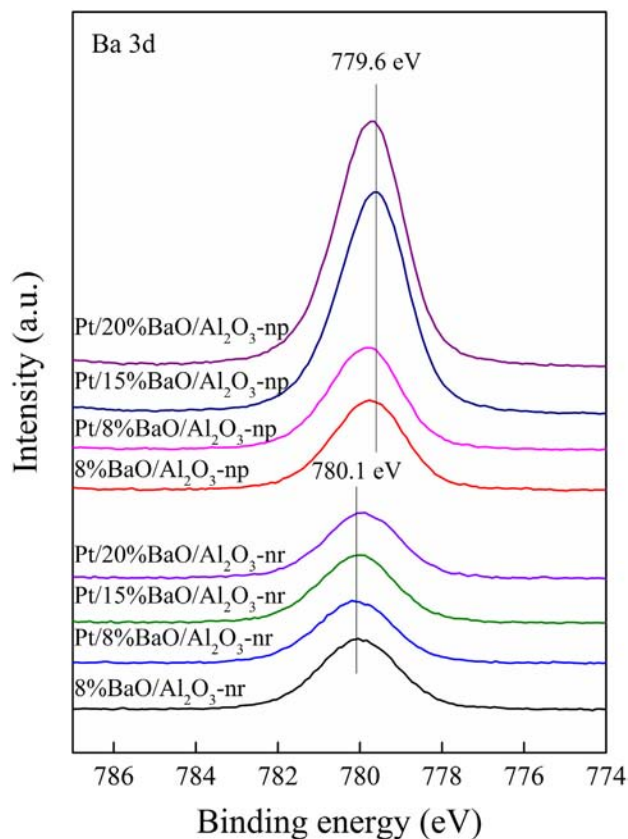
Fig. 6 – XPS Ba 3d 5/2 spectra for 8%BaO/Al$_2$O$_3$ and Pt/BaO/Al$_2$O$_3$ catalysts.

suggests that both the metallic and oxidized states coexisted over the NSR catalysts, with similar high dispersion.

As shown in Fig. 6, interestingly, the XPS spectra of Ba 3d exhibited a strong support dependence. In the case of the NSR samples prepared from Al$_2$O$_3$-nr, the Ba 3d 5/2 peaks showed binding energies at 780.1 eV, indicating that the Ba-containing component was in the form of BaCO$_3$ (Gauzzi et al., 1990) and further confirming the results of XRD. In contrast with the samples prepared from Al$_2$O$_3$-nr, a negative binding energy shift of Ba of about 0.5 eV was observed over the catalysts derived from Al$_2$O$_3$-np, and also for the BaO/Al$_2$O$_3$-np sample. These results strongly suggest that Al$_2$O$_3$-nr is more electrophilic than Al$_2$O$_3$-np, with donation of higher electron density from the Ba 3d band to the support (Olsson and Fridell, 2002). In other words, a strong interaction between the Ba-containing phase and support was present for the Al$_2$O$_3$-nr related NSR samples.

As for all the NSR catalysts prepared from Al$_2$O$_3$-nr, it should be noted that the intensity of the Ba peak was almost the same regardless of their quite different loadings. In the case of the samples derived from Al$_2$O$_3$-np, however, increased BaO loading always resulted in a stronger intensity for the Ba 3d peak. For a given BaO content, meanwhile, Pt/BaO/Al$_2$O$_3$-np exhibited a Ba peak of much stronger intensity than the corresponding one prepared from Al$_2$O$_3$-nr, indicating that a higher surface concentration of Ba species was present for the Pt/BaO/Al$_2$O$_3$-np. As shown in Fig. 3, however, the Pt/BaO/Al$_2$O$_3$-np samples always showed a lower NSC value than the

Pt/BaO/Al$_2$O$_3$-nr materials with the same BaO loading. With this in mind, one can deduce that it is not the surface concentration of Ba species but other factors governing the NO$_x$ storage capacity. To address this issue, H$_2$-TPR experiments were performed for all the samples.

Fig. 7 shows the H$_2$-TPR profiles of the series of Pt/BaO/Al$_2$O$_3$ catalysts, along with samples containing only one active component (1 wt.% Pt or 8 wt.% BaO). It can be seen from the Pt/Al$_2$O$_3$ samples (Fig. 7) that the peaks at 200 and 360°C with low intensity can be assigned to the reduction of platinum oxide (Dong et al., 2017; Luo et al., 2008). During the H$_2$-TPR process performed over the BaO/Al$_2$O$_3$ (Fig. 7), two weak H$_2$ consumption peaks were detected around 360 and 520–560°C, respectively, which originated from the reduction of Ba compounds (Dong et al., 2017; Luo et al., 2008).

On all Pt/BaO/Al$_2$O$_3$ catalysts, except Pt/8%BaO/Al$_2$O$_3$-np, a much stronger H$_2$ consumption peak appeared at moderate temperatures centered at 455–470°C compared with the samples only containing one active component. The higher the BaO loading, the larger the amount of H$_2$ consumption. These results strongly suggest that the coexistence of Pt and Ba components dramatically enhanced the reducibility of the NSR samples, the occurrence of which can be explained by the following reasons. Over Pt/BaO/Al$_2$O$_3$, previous studies proposed that the presence of Ba species increased the fraction of oxidized Pt species (Castoldi et al., 2004; Olsson and Fridell, 2002), giving more PtO$_x$ able to react with H$_2$. In our case, however, all the NSR samples
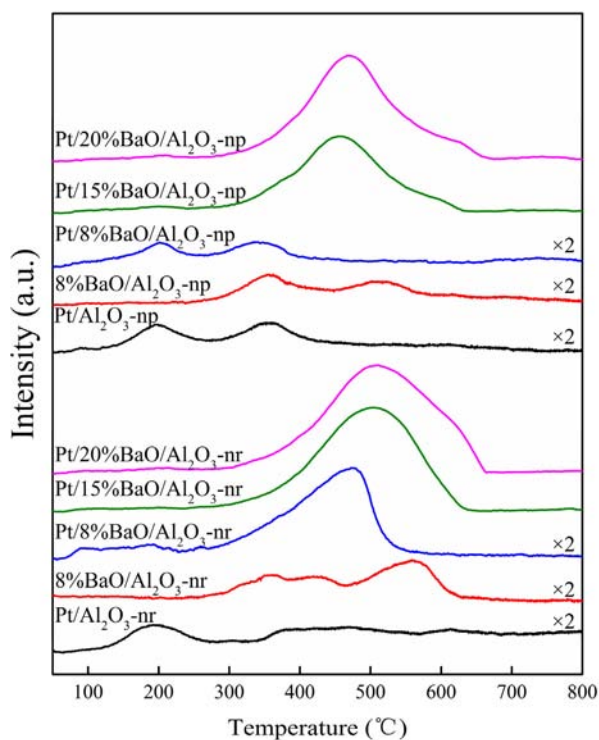
Fig. 7 – H$_2$ temperature programmed reduction (H$_2$-TPR) profiles of Pt/Al$_2$O$_3$, 8%BaO/Al$_2$O$_3$, and Pt/BaO/Al$_2$O$_3$ catalysts.

exhibited Pt 4d peaks with almost the same binding energy and intensity (Fig. 5), while these samples gave quite different reducibility (Fig. 7). This result suggests that the difference in the chemical state of Pt (metallic or oxidized states) is not the main reason contributing to the distinct difference in H$_2$-TPR profiles. It is easily found from Fig. 6 that a much higher concentration of BaCO$_3$ was present on the surface of Pt/BaO/Al$_2$O$_3$-np compared with Pt/BaO/Al$_2$O$_3$-nr with the same Ba loading, while a much smaller amount of H$_2$ was consumed in the former sample (Fig. 7). As a result, it is reasonable that the surface concentration of Ba-containing species does not govern the reducibility of NSR catalysts. Previous studies have revealed that intimate contact between Pt- and Ba-containing species is required for the reduction of nitrates to occur on Pt/BaO/Al$_2$O$_3$ catalysts (Hu et al., 2013; Yi et al., 2007; Zhou et al., 2006), by promoting reverse spillover of nitrates from the Ba sites to the Pt surface. With this in mind, such intimate contact may also enhance the spillover of H$_2$ between Ba and Pt components, improving the reducibility of NSR catalysts (Zhang et al., 2016).

For a given BaO loading, the Al$_2$O$_3$-nr supported NSR sample always gave a much stronger H$_2$ consumption peak than the corresponding one prepared from Al$_2$O$_3$-np, even though a higher concentration of Ba species was present on the surface of the former sample. These results indicate that the interaction between Ba and Pt species on the Al$_2$O$_3$-nr is much stronger, giving more sites available for reaction with H$_2$. For the Al$_2$O$_3$-nr supported sample, this stronger interaction results in more difficult-to-reduce species (Kikuyama et al., 2002; Nova et al., 2004). As a result, it is reasonable that the H$_2$ consumption peak appeared at a higher temperature compared with the corresponding Pt/BaO/Al$_2$O$_3$-np sample with the same BaO loading.

2.4. Reaction sites and mechanism evaluated by *in situ* DRIFTS

The behavior of NSR catalysts in the NO$_x$ storage and reduction processes was evaluated by *in situ* DRIFTS at 300°C, with typical results shown in Fig. 8 and Appendix A Fig. S4. After exposing Pt/15%BaO/Al$_2$O$_3$-nr to NO + O$_2$ for 1 min (Fig. 8a and Appendix A Fig. S4), bands at 1232 and 1312 cm^{-1} were clearly observed, assigned to bridging nitrite on Ba and/or Al sites (Muncrief et al., 2004; Prinetto et al., 2001; Sedlmair et al., 2003; Su and Amiridis, 2004). This result indicates that a nitrite route occurred during the initial stage of NO$_x$ storage (Nova et al., 2004; Sedlmair, 2003), and in that case a cooperative interaction between Pt and a neighboring Ba site is crucial for nitrite formation. Meanwhile, the appearance of a band at 1546 cm^{-1} indicated the formation of bidentate nitrate on Al in proximity to a Ba site (Westerberg and Fridell, 2001), confirming the simultaneous occurrence of a nitrate pathway involving the oxidation of NO to NO$_2$ on the Pt site (Nova et al., 2004; Sedlmair, 2003). After 2 min, a shoulder at 1324 cm^{-1} was observed, together with a weak band at 1394 cm^{-1}, indicative of the appearance of monodentate nitrate linked with Ba (Sedlmair, 2003). These results clearly show that Ba-Pt and Ba-Al neighboring sites are essential for triggering the formation of ad-NO$_x$ species and for their spillover (Castoldi et al., 2004; Piacentini et al., 2005; Zhou et al., 2006). As time went on, the intensity of peaks due to nitrates (1555, 1394, 1324, and 1250 cm^{-1}) increased significantly. Increased intensity was also observed for the nitrite species (1312 and 1232 cm^{-1}), while at a lower rate than nitrates. This trend was evident from change in the peak at 1232 cm^{-1}, which firstly increased gradually within 3 min, and was subsequently overlapped by a new band at 1250 cm^{-1} arising from nitrate (Westerberg and Fridell, 2001). During this process, meanwhile, the oxidation of nitrites to nitrate species would occur on the catalyst surface (Liotta et al., 2002; Sedlmair, 2003). As a result, it is reasonable that the nitrates were predominant during the final stage of NO$_x$ storage.

After switched the feed gas to H$_2$ + N$_2$ (Fig. 8b), nitrate linked with Al sites (1555 and 1250 cm^{-1}) decreased more rapidly than nitrate trapped on Ba sites (1394 and 1330 cm^{-1}). Within 80 sec, the nitrate adsorbed on Al sites disappeared, while complete removal of nitrate from Ba sites occurred in 120 sec. These results indicate that nitrate bound on Al sites has higher activity due to the lower alkalinity of Al than Ba (Sedlmair, 2003).

The DRIFT spectra of the NO$_x$ storage and reduction processes on Pt/15%BaO/Al$_2$O$_3$-np are shown in Fig. 8c and d. As with the nanorod samples, bridging nitrite on Al and/or Ba sites (1232 and 1307 cm^{-1}) was formed as soon as the catalyst was exposed to NO + O$_2$ for 1 min. With increasing reaction time, nitrates on Al (1546 and 1250 cm^{-1}) and on Ba (1394 and 1326 cm^{-1}) appeared and became predominant after 30 min. Different from the nr samples, one broad peak between 1430 and 1490 cm^{-1} was observed, indicating the formation of bulk nitrates (or ionic nitrates) on Pt/15%BaO/Al$_2$O$_3$-np (Wu et al., 2014). When exposing Pt/15%BaO/Al$_2$O$_3$-np to a reducing atmosphere (Fig. 8d), the nitrate on Al sites decreased quickly in the first 60 sec, which was followed by a sharp decrease of nitrate on Ba sites (this mainly occurred between 60 and 100 sec). Even after 120 sec, it should be noted that a weak band at 1430–1490 cm^{-1} was still observed, indicating the lower
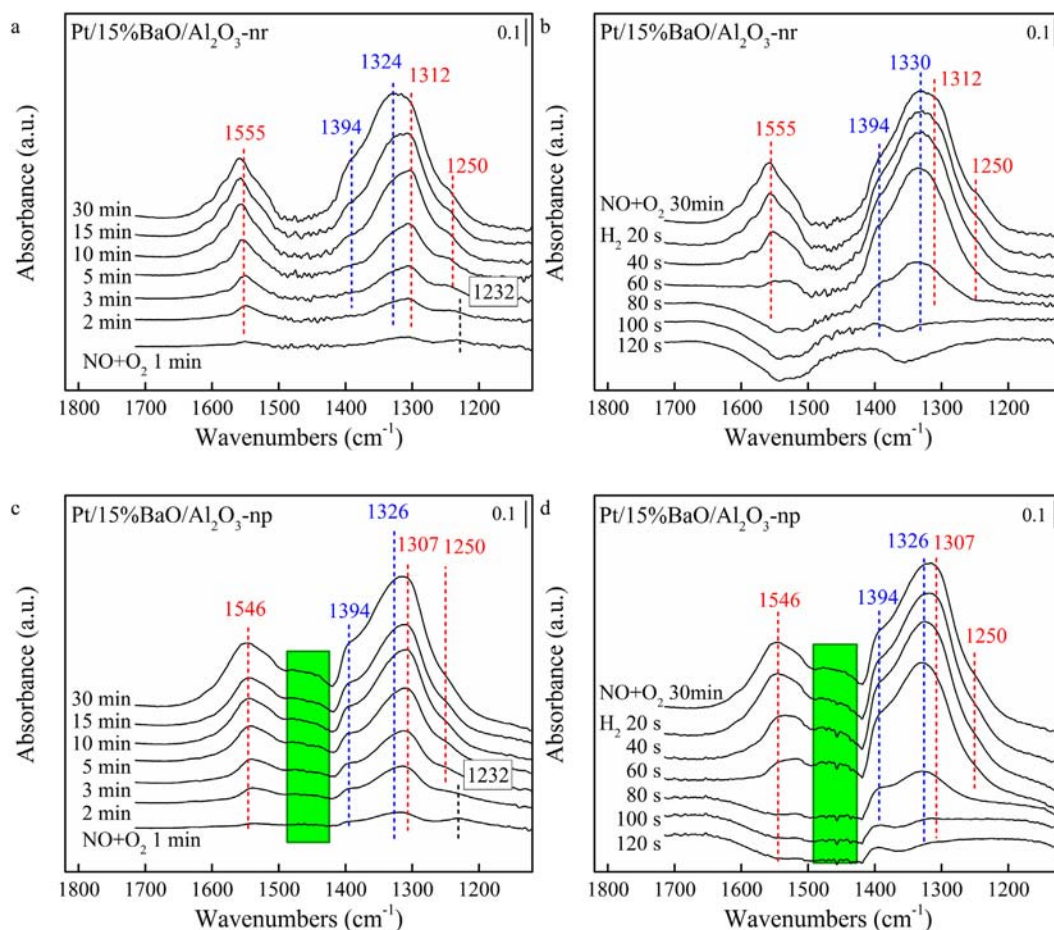
Fig. 8 – *In situ* diffuse reflectance infrared Fourier transform spectroscopy (DRIFTS) spectra of Pt/15%BaO/Al$_2$O$_3$-nr during (a) storage and (b) reduction processes at 300°C, and of Pt/15%BaO/Al$_2$O$_3$-np during (c) storage and (d) reduction processes at 300°C.

activity of bulk nitrates species than surface-bound species. This may serve as an explanation for the lower NO$_x$ conversion efficiency of Pt/nBaO/Al$_2$O$_3$-np. The appearance of bulk nitrates revealed the existence of large Ba-containing particles, which exhibited high stability during the lean phase and low activity for NO$_x$ release when reductants were introduced (Prinetto et al., 2001; Rodrigues et al., 2001).

2.5. Relationship between the structure of NSR catalysts and their catalytic performance

As shown in Fig. 3, the NSR catalysts derived from Al$_2$O$_3$ nanorods exhibited much higher NO$_x$ storage capacity than the samples prepared from Al$_2$O$_3$ particles. Such strong dependence on support morphology was also observed during the lean/rich cyclic operation (Fig. 4). The Pt/BaO/Al$_2$O$_3$-nr materials has a lower BET surface area than the corresponding Pt/BaO/Al$_2$O$_3$-np samples with the same BaO loading, indicating that this property is not the key factor governing the NSR behavior of Pt/BaO/Al$_2$O$_3$. Over these two kinds of samples, the *in situ* DRIFTS study revealed that the nitrite route and the nitrate pathway simultaneously occurred during the initial stage of the NO$_x$ storage process (Fig. 8). As for Pt/BaO/Al$_2$O$_3$, previous

studies revealed that intimate contact of Ba-Al and Ba-Pt sites was essential for triggering both routes (Castoldi et al., 2004; Piacentini et al., 2005; Zhou et al., 2006).

For all the Pt/BaO/Al$_2$O$_3$ samples, XRD and XPS measurements confirmed that the Ba species was present in the form of BaCO$_3$ (Figs. 2 and 6). However, it should be pointed out that the Ba binding energy of Pt/BaO/Al$_2$O$_3$-nr was always ca. 0.5 eV higher than that of Pt/BaO/Al$_2$O$_3$-np, indicating a stronger interaction between BaCO$_3$ and the Al$_2$O$_3$-nr support. Compared with BaO/Al$_2$O$_3$-np, such a shift of Ba binding energy toward higher values was also observed for BaO/Al$_2$O$_3$-nr, which further confirmed the strong interaction between the Ba phase and support regardless of the presence of Pt. The stronger interaction between Ba-containing species and Al$_2$O$_3$ nanorods may also promote the dispersion of Ba. As a result, it is reasonable that the particle size of BaCO$_3$ on Pt/BaO/Al$_2$O$_3$-nr was always smaller than for the corresponding sample prepared from Al$_2$O$_3$-np with the same BaO loading (Table 1), giving more active sites for the NSR process.

In principle, nanomaterials with different shapes are enclosed by different facets, on which the atomic arrangement and coordination status are also quite distinct from each other (Li and Shen, 2014). As a result, different interactions would be

achieved if hetero-atoms were introduced onto nanomaterials with different shapes. This situation would occur during preparation of NSR catalysts using Al_2O_3 nanorods or nanoparticles as the support, considering that the coordination features of Al^{3+} ions are closely related to the exposed crystal surface of Al_2O_3 (Digne et al., 2002; Kwak et al., 2007, 2009). To reveal the intrinsic properties governing the correlation between the support morphology and the dispersion of Ba, the exposed crystal surfaces of Al_2O_3-nr and Al_2O_3-np should be characterized carefully.

For all the NSR samples, XPS measurements showed that the surface concentration of Pt was almost the same. XPS analysis also revealed that a much higher amount of Ba was present on the surface of Pt/BaO/Al_2O_3-np compared with that of Pt/BaO/Al_2O_3-nr with the same BaO loading. In contrast, the Pt/BaO/Al_2O_3-nr samples exhibited a much stronger H_2 consumption peak than the corresponding materials derived from Al_2O_3-np. These results strongly suggest that intimate contact between Ba-Pt sites was present for the Al_2O_3-nr related NSR samples, benefiting H_2 spillover and improving the reducibility of the NSR catalysts (Zhang et al., 2016). A previous study carried out by Hu et al. (2013) revealed that for Pt/BaO/Al_2O_3 catalysts, an increase in the crystallinity of Al_2O_3 would increase the proximity of Pt to BaO sites, leading to much more efficient NSR performance. With this in mind, it is also reasonable that stronger intimate contact between Ba-Pt sites was present for the Pt/BaO/Al_2O_3-nr catalysts, due to the higher crystallinity of Al_2O_3-nr than Al_2O_3-np (Fig. 2).

Clearly, intimate contact of Ba-Al and Ba-Pt sites was achieved on Pt/BaO/Al_2O_3 when using Al_2O_3-nr as a support. Such shape dependence for the support thus afforded a higher NO_x storage capacity for Pt/BaO/Al_2O_3-nr, by accelerating the formation of surface nitrites and nitrates and also their spillover during lean conditions. Under rich conditions, meanwhile, this strong interaction of the multi-components of Pt/BaO/Al_2O_3-nr was beneficial for the reverse spillover of ad-NO_x species onto the Pt surface, enhancing their reduction (Anderson et al., 2003; Hu et al., 2013; Maeda et al., 2011). As a result, a lower NO_x spike was always observed for Pt/BaO/Al_2O_3-nr during the rich periods, leading to a higher average NO_x conversion than that of Pt/BaO/Al_2O_3-np.

3. Conclusions

The morphology of the alumina support was found to have a significant effect on the catalytic performance of Pt/BaO/Al_2O_3. The Pt/BaO/Al_2O_3 materials prepared from Al_2O_3 nanorods exhibited much higher NO_x storage capacity under lean conditions compared with corresponding samples derived from Al_2O_3 particles, and also gave higher NO_x removal efficiency during rich-lean cyclic operation. XRD and XPS measurements confirmed that stronger interaction between Ba-containing species and Al_2O_3 was achieved by employing Al_2O_3-nr as a support for Pt/BaO/Al_2O_3 preparation. H_2-TPR and XPS analysis revealed that intimate contact between Pt and neighboring Ba was present on the Al_2O_3-nr related NSR samples. Such strong interaction among the multi-components of Pt/BaO/Al_2O_3-nr thus accelerated the formation of surface nitrite and nitrate during the NO_x storage

process, the occurrence of which has been confirmed by *in situ* DRIFTS measurements. Under rich conditions, the intimate contact of Ba-Pt and Ba-Al sites promoted the reverse spillover of ad-NO_x species onto the Pt surface, enhancing their reduction. These findings may be fundamental for designing NSR catalysts with high catalytic performance.

Acknowledgments

Appendix A. Supplementary material

REFERENCES

Amberntsson, A., Fridell, E., Skoglundh, M., 2003. Influence of platinum and rhodium composition on the NOx storage and Sulphur tolerance of a barium based NOx storage catalyst. Appl. Catal. B Environ. 46, 429–439.

Anderson, J.A., Bachiller-Baeza, B., Fernández-García, M., 2003. Role of Pt in Pt/Ba/Al₂O₃ NOx storage and reduction traps. Phys. Chem. Chem. Phys. 5, 4418–4427.

Bhatia, D., McCabe, R.W., Harold, M.P., Balakotaiah, V., 2009. Experimental and kinetic study of NO oxidation on model Pt catalysts. J. Catal. 266, 106–119.

Burch, R., 2011. Knowledge and know-how in emission control for mobile applications. Catal. Rev. 46, 271–334.

Castoldi, L., Nova, I., Lietti, L., Forzatti, P., 2004. Study of the effect of Ba loading for catalytic activity of Pt-Ba/Al₂O₃ model catalysts. Catal. Today 96, 43–52.

Clayton, R.D., Harold, M.P., Balakotaiah, V., Wan, C.Z., 2009. Pt dispersion effects during NOx storage and reduction on Pt/BaO/Al₂O₃ catalysts. Appl. Catal. B Environ. 90, 662–676.

Cui, Y., Yan, Q., Zhang, C., Qiu, L., Wang, Q., 2017. Pt/Ba/Co₁Mg₂Al₁Ox with dual adsorption sites: a novel NOx storage and reduction catalyst. Catal. Commun. 101, 125–128.

Digne, M., Sautet, P., Raybaud, P., Euzen, P., Toulhoat, H., 2002. Hydroxyl groups on γ-alumina surfaces: a DFT study. J. Catal. 211, 1–5.

Dong, M., Wang, J., Zhu, J., Wang, J., Wang, W., Shen, M., 2017. Effects of Pd doping on N₂O formation over Pt/BaO/Al₂O₃ during NOx storage and reduction process. Front. Environ. Sci. Eng. 11, 11.

Epling, W.S., Campbell, L.E., Yezerets, A., Currier, N.W., Parks, J.E., 2004. Overview of the fundamental reactions and degradation mechanisms of NOx storage/reduction catalysts. Catal. Rev. 46, 163–245.

Epling, W.S., Yezerets, A., Currier, N.W., 2007. The effects of regeneration conditions on NOx and NH₃ release from NOx storage/reduction catalysts. Appl. Catal. B Environ. 74, 117–129.

Fridell, E., Persson, H., Westerberg, B., Olsson, L., Skoglundh, M., 2000. The mechanism for NOx storage. Catal. Lett. 66, 71–74.

Gauzzi, A., Mathieu, H.J., James, J.H., Kellett, B., 1990. AES, XPS and SIMS characterization of YBa₂Cu₃O₇ superconducting high T꜀ thin films. Vacuum 41, 870–874.

Hu, Z., Li, W.Z., Sun, K.Q., Xu, B.Q., 2013. Effects of support pre-calcination on the NOx storage and reduction performance of Pt-BaO/Al$_2$O$_3$ catalysts. Catal. Sci. Technol. 3, 2062–2071.

Huang, B., Yu, D., Sheng, Z., Yang, L., 2017. Novel CeO$_2$@TiO$_2$ core-shell nanostructure catalyst for selective catalytic reduction of NOx with NH$_3$. J. Environ. Sci. 55, 129–136.

Hussam, A., Erik, F., Magnus, S., 2004. Influence of the type of reducing agent (H$_2$, CO, C$_3$H$_6$ and C$_3$H$_8$) on the reduction of stored NOx in a Pt/BaO/Al$_2$O$_3$ model catalyst. Top. Catal. 30-31, 161–168.

Hussam, A., Erik, F., Magnus, S., 2006. The reduction phase in NOx storage catalysis: effect of type of precious metal and reducing agent. Appl. Catal. B Environ. 62, 319–328.

Ji, Y., Choi, J.S., Toops, T.J., Crocker, M., Naseri, M., 2008. Influence of ceria on the NOxstorage/reduction behavior of lean NOx trap catalysts. Catal. Today 136, 146–155.

Kašpar, J., Fornasiero, P., Hickey, N., 2003. Automotive catalytic converters: current status and some perspectives. Catal. Today 77, 419–449.

Kikuyama, S., Matsukuma, I., Kikuchi, R., Sasaki, K., Eguchi, K., 2002. A role of components in Pt-ZrO$_2$/Al$_2$O$_3$ as a sorbent for removal of NO and NO$_2$. Appl. Catal. A Gen. 226, 23–30.

Kim, J.G., Lee, H.M., Lee, M.J., Lee, J.H., Kim, J.G., Jeon, J.Y., et al., 2008. Effect of Co and Rh promoter on NOx storage and reduction over Pt/BaO/Al$_2$O$_3$ catalyst. J. Ind. Eng. Chem. 14, 841–846.

Kim, D.H., Mudiyanselage, K., Szanyi, J., Kwak, J.H., Zhu, H., Peden, C., 2013. Effect of K loadings on nitrate formation/decomposition and on NOx storage performance of K-based NOx storage-reduction catalysts. Appl. Catal. B Environ. 142-143, 472–478.

Kwak, J., Hu, J., Kim, D., Szanyi, J., Peden, C., 2007. Penta-coordinated Al^{3+} ions as preferential nucleation sites for BaO on γ-Al$_2$O$_3$: an ultra-high-magnetic field ^{27}Al MAS NMR study. J. Catal. 251, 189–194.

Kwak, J., Mei, D., Yi, C., Kim, D., Peden, C., Allard, L., et al., 2009. Understanding the nature of surface nitrates in BaO/γ-Al$_2$O$_3$ NOx storage materials: a combined experimental and theoretical study. J. Catal. 261, 17–22.

Li, Y., Shen, W., 2014. Morphology-dependent nanocatalysts: rod-shaped oxides. Chem. Soc. Rev. 43, 1543–1574.

Liotta, L.F., Macaluso, A., Arena, G.E., Livi, M., Centi, G., Deganello, G., 2002. A study of the behaviour of Pt supported on CeO$_2$-ZrO$_2$/Al$_2$O$_x$-BaO as NOx storage-reduction catalyst for the treatment of lean burn engine emissions. Catal. Today 75, 439–449.

Liu, G., Gao, P.-X., 2011. A review of NOx storage/reduction catalysts: mechanism, materials and degradation studies. Catal. Sci. Technol. 1, 552–568.

Liu, Z., Woo, S.I., 2006. Recent advances in catalytic DeNOxscience and technology. Catal. Rev. 48, 43–89.

Luo, J.Y., Meng, M., Zha, Y.Q., Xie, Y.N., Hu, T.D., Zhang, J., et al., 2008. A comparative study of Pt/Ba/Al$_2$O$_3$ and Pt/Fe-Ba/Al$_2$O$_3$ NSR catalysts: new insights into the interaction of Pt-Ba and the function of Fe. Appl. Catal. B Environ. 78, 38–52.

Lv, L., Wang, X., Shen, M., Zhang, Q., Wang, J., 2013. The lean NOx traps behavior of (1-5%) BaO/CeO$_2$ mixed with Pt/Al$_2$O$_3$ at low temperature (100–300 °C): the effect of barium dispersion. Chem. Eng. J. 222, 401–410.

Maeda, N., Urakawa, A., Baiker, A., 2009. Support effects and chemical gradients along the catalyst bed in NOx storage-reduction studied by space- and time-resolved in situ DRIFTS. J. Phys. Chem. C 113, 16724–16735.

Maeda, N., Urakawa, A., Sharma, R., Baiker, A., 2011. Influence of Ba precursor on structural and catalytic properties of Pt-Ba/alumina NOx storage-reduction catalyst. Appl. Catal. B Environ. 103, 154–162.

Matsumoto, S., 2004. Recent advances in automobile exhaust catalysts. Catal. Today 90, 183–190.

Miyoshi, N., Matsumoto, S., Katoh, K., Tanaka, T., Harada, J., Takahashi, N., et al., 1995. Development of new concept three-way catalyst for automotive lean-burn engines. SAE paper: 950809.

Muncrief, R.L., Khanna, P., Kabin, K.S., Harold, M.P., 2004. Mechanistic and kinetic studies of NOx storage and reduction on Pt/BaO/Al$_2$O$_3$. Catal. Today 98, 393–402.

Nova, I., Castoldi, L., Lietti, L., Tronconi, E., Forzatti, P., Prinetto, F., et al., 2004. NOx adsorption study over Pt-Ba/alumina catalysts: FT-IR and pulse experiments. J. Catal. 222, 377–388.

Olsson, L., Fridell, E., 2002. The influence of Pt oxide formation and Pt dispersion on the reactions NO$_2$ ⇔ NO+1/2 O$_2$ over Pt/Al$_2$O$_3$ and Pt/BaO/Al$_2$O$_3$. J. Catal. 210, 340–353.

Olsson, L., Persson, H., Fridell, E., Skoglundh, M., Andersson, B., 2001. A kinetic study of NO oxidation and NOx storage on Pt/Al$_2$O$_3$ and Pt/BaO/Al$_2$O$_3$. J. Phys. Chem. B 105, 6895–6906.

Piacentini, M., Maciejewski, M., Baiker, A., 2005. Pt-Ba/alumina NOx storage-reduction catalysts: effect of Ba-loading on build-up, stability and reactivity of Ba-containing phases. Appl. Catal. B Environ. 59, 187–195.

Prinetto, F., Ghiotti, G., Nova, I., Lietti, L., Tronconi, E., Forzatti, P., 2001. FT-IR and TPD investigation of the NOx storage properties of BaO-Al$_2$O$_3$ and Pt-BaO/Al$_2$O$_3$ catalysts. J. Phys. Chem. B 105, 12732–12745.

Rao, M.P., Wu, J.J., Asiri, A.M., Anandan, S., Ashokkumar, M., 2018. Photocatalytic properties of hierarchical CuO nanosheets synthesized by a solution phase method. J. Environ. Sci. 69, 115–124.

Rodrigues, F., Juste, L., Potvin, C., Tempère, J.F., Blanchard, G., Djéga-Mariadassou, G., 2001. NOx storage on barium-containing three-way catalyst in the presence of CO$_2$. Catal. Lett. 72, 59.

Roy, S., Baiker, A., 2009. NOx storage-reduction catalysis: from mechanism and materials properties to storage-reduction performance. Chem. Rev. 109, 4054–4091.

Say, Z., Dogac, M., Vovk, E.I., Kalay, Y.E., Kim, C.H., Li, W., et al., 2014. Palladium doped perovskite-based NO oxidation catalysts: the role of Pd and B-sites for NOx adsorption behavior via in-situ spectroscopy. Appl. Catal. B Environ. 154-155, 51–61.

Sedlmair, Ch., Seshan, K., Jentys, A., Lercher, J.A., 2003. Elementary steps of NOx adsorption and surface reaction on a commercial storage-reduction catalyst. J. Catal. 214, 308–316.

Su, Y., Amiridis, M.D., 2004. In situ FTIR studies of the mechanism of NOx storage and reduction on Pt/Ba/Al$_2$O$_3$ catalysts. Catal. Today 96, 31–41.

Wang, X., Yu, Y., He, H., 2010. Effect of Co addition to Pt/Ba/Al$_2$O$_3$ system for NOx storage and reduction. Appl. Catal. B Environ. 100, 19–30.

Wang, X., Yu, Y., He, H., 2011. Effects of temperature and reductant type on the process of NOx storage reduction over Pt/Ba/CeO$_2$ catalysts. Appl. Catal. B Environ. 104, 151–160.

Wang, L., He, H., Zhang, C., Sun, L., Liu, S., Wang, S., 2016. Antimicrobial activity of silver loaded MnO$_2$ nanomaterials with different crystal phases against Escherichia coli. J. Environ. Sci. 41, 112–120.

Westerberg, B., Fridell, E., 2001. A transient FTIR study of species formed during NOx storage in the Pt/BaO/Al$_2$O$_3$ system. J. Mol. Catal. A Chem. 165, 249–263.

Wu, D.L., Tschamber, V., Limousy, L., Michelin, L., Westermann, A., Azambre, B., et al., 2014. Combined fixed-bed reactor and in situ DRIFTS tests of NO adsorption on a NOx storage-reduction system catalyst. Chem. Eng. Technol. 37, 204–212.

Yi, C.W., Kwak, J.H., Peden, C.H.F., Wang, C., Szanyi, J., 2007. Understanding practical catalysts using a surface science approach:the importance of strong interaction between BaO and Al$_2$O$_3$ in NOxstorage materials. J. Phys. Chem. B 111, 14942–14944.

Zhang, Z.S., Chen, B.B., Wang, X.K., Xu, L., Au, C., Shi, C., et al., 2015. NOx storage and reduction properties of model

manganese-based lean NOx trap catalysts. Appl. Catal. B Environ. 165, 232–244.

Zhang, Y., Yu, Y., He, H., 2016. Oxygen vacancies on nanosized ceria govern the NOx storage capacity of NSR catalysts. Catal. Sci. Technol. 6, 3950–3962.

Zhou, K., Li, Y., 2012. Catalysis based on nanocrystals with well-defined facets. Angew. Chem. Int. Ed. 51, 602–613.

Zhou, G., Luo, T., Gorte, R.J., 2006. An investigation of NOx storage on Pt-BaO-Al$_2$O$_3$. Appl. Catal. B Environ. 64, 88–95.